JACS
JOURNAL OF THE AMERICAN CHEMICAL SOCIETY

ARTICLE

pubs.acs.org/JACS

DNP by Thermal Mixing under Optimized Conditions Yields >60 000-fold Enhancement of ^{89}Y NMR Signal

Lloyd Lumata,[†] Ashish K. Jindal,[†] Matthew E. Merritt,[†] Craig R. Malloy,[†] A. Dean Sherry,[†,‡] and Zoltan Kovacs*[,†]

[†]Advanced Imaging Research Center, University of Texas Southwestern Medical Center, 5323 Harry Hines Boulevard, Dallas, Texas 75390, United States

[‡]Department of Chemistry, University of Texas, Dallas, 800 West Campbell Road, Richardson, Texas 75080, United States

Supporting Information

ABSTRACT: Hyperpolarized ^{89}Y complexes are attractive NMR spectroscopy and MR imaging probes due to the exceptionally long spin−lattice relaxation time ($T_1 \approx 10$ min) of the ^{89}Y nucleus. However, *in vivo* imaging of ^{89}Y has not yet been realized because of the low NMR signal enhancement levels previously achieved for this ultra low-γ_n nucleus. Here, we report liquid-state ^{89}Y NMR signal enhancements over 60 000 times the thermal signal at 298 K in a 9.4 T magnet, achieved after the dynamic nuclear polarization (DNP) of Y(III) complex of 1,4,7,10-tetraazacyclododecane-1,4,7,10-tetraacetic acid (DOTA) samples at 3.35 T and 1.4 K. The ^{89}Y DNP was shown to proceed by thermal mixing and the liquid state ^{89}Y NMR signal enhancement was maximized by (*i*) establishing the optimal microwave irradiation frequency, (*ii*) optimizing the glassing matrix, (*iii*) choosing a radical with negligible inhomogeneous line broadening contribution to the ESR linewidth, and (*iv*) addition of an electron T_{1e} relaxation agent. The highest enhancements were achieved using a trityl OX063 radical combined with a gadolinium relaxation agent in water-glycerol matrix. Co-polarization of ^{89}YDOTA and sodium [1-^{13}C]pyruvate showed that both ^{89}Y and ^{13}C nuclear species acquired the same spin temperature, consistent with thermal mixing theory of DNP. This methodology may be applicable for the optimization of DNP of other low-γ_n nuclei.

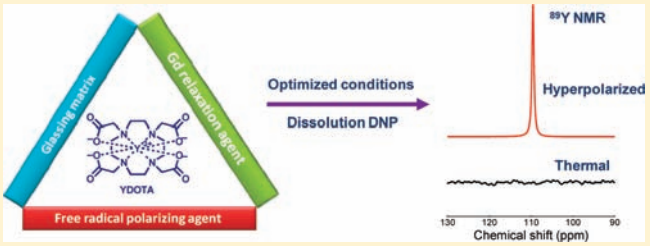

INTRODUCTION

Nuclear magnetic resonance (NMR) spectroscopy is one of the most important structure elucidation techniques in chemistry and biochemistry. NMR is also the underlying principle of magnetic resonance imaging (MRI), an important clinical imaging modality that can noninvasively provide exquisite high resolution images of soft tissues throughout the body. The NMR signal intensity depends on the nuclear spin polarization P which is the proportional to the surplus number of nuclear spins in a Zeeman energy level. In thermal equilibrium, the nuclear spin population distribution is governed by the Boltzmann statistics and P is given by the Brillouin function which, for a spin-1/2 system, is written as $P = \tanh(\mu B/kT)$ where μ is the magnetic moment, B is the applied magnetic field, k is the Boltzmann constant, and T is the temperature.[1,2] The magnetic moment μ of a nucleus with a spin quantum number I is given by $\mu = \gamma_n \hbar I$ where γ_n is the gyromagnetic ratio and $\hbar$ is the Planck's constant divided by 2π. Since at ambient conditions the magnetic energy μB of the nuclear spins is much lower than its thermal energy kT, NMR has inherently low sensitivity which particularly hampers magnetic resonance spectroscopy and imaging of nuclei with low γ_n.[3−5]

Dynamic nuclear polarization (DNP) offers an elegant solution to this low-sensitivity problem by creating a nonthermal equilibrium spin state population of the observed nuclei. The sample containing the target nuclei is typically doped with a paramagnetic species (organic free radicals or paramagnetic metal complexes) in a glassing matrix. DNP is achieved by transferring the high electron thermal polarization (due to the robust electronic gyromagnetic ratio $\gamma_e \approx 28\,000$ MHz/T) to the nuclear spins at low temperature (close to 1 K) and in high magnetic field (>1 T) via microwave irradiation near the electron resonance frequency.[3−5] Until recently, the DNP technology has been used exclusively for production of polarized targets for nuclear and particle physics experiments.[3−5] The technique gained practical importance in chemistry and biomedical imaging when it was shown by the pivotal work of Golman and Ardenkjaer-Larsen[6] that the frozen polarized sample can be dissolved using a fast-dissolution method to produce solutions containing highly polarized (hyperpolarized) ^{13}C and ^{15}N-labeled compounds that can be used for *in vitro* and *in vivo* NMR spectroscopy and imaging at physiological temperatures.[6−18]

^{89}Y (I = 1/2, γ_n = 2.0864 MHz/T, 100% natural isotopic abundance) is an attractive nucleus for the design of responsive

Received: March 1, 2011
Published: May 04, 2011

dx.doi.org/10.1021/ja201880y | *J. Am. Chem. Soc.* 2011, 133, 8673–8680

Chart 1. Structure of YDOTA

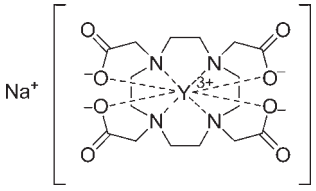

magnetic resonance spectroscopy and imaging probes because of the sensitivity of the ^{89}Y NMR chemical shift to the coordination environment of the Y(III) ion. This sensitivity has been exploited in the design of ^{89}Y NMR probes to study protein structure[20] and to report pH.[21] However, unlike proton, ^{89}Y has a very low γ_n, and consequently, at ambient temperature an ensemble of ^{89}Y spins in thermal equilibrium has extremely low nuclear polarization ($P = 1.578 \times 10^{-4}$ % at 9.4 T and 298 K). This low thermal polarization, combined with a long nuclear spin−lattice relaxation time T_1, makes ^{89}Y one of the most challenging nuclei for conventional NMR and MRI.

Recently, we have shown that various ^{89}Y complexes such as YDOTA (Chart 1) can be hyperpolarized with commercially available hardware using the trityl radical OX063 as the polarizing agent.[19,21] In preliminary experiments,[19,21] we achieved only modest ^{89}Y signal enhancements (up to 3000 over thermal equilibrium at 310 K) that were not sufficient for imaging applications. Therefore, the goal of the present work was to optimize the experimental parameters associated with DNP of ^{89}Y to achieve a polarization level that would enable us to perform *in vivo* imaging of hyperpolarized yttrium complexes.[19,21,22] Here we show that we can enhance the room-temperature NMR signal of ^{89}Y up to 65 000 times the thermal signal via the fast-dissolution DNP technique. This is significant progress toward developing hyperpolarized ^{89}Y-complexes as *in vivo* NMR and MRI probes where, in this case, the long T_1 of ^{89}Y translates into a long polarization lifetime allowing the observation of biological processes occurring on a longer time scale.

EXPERIMENTAL METHODS

Materials. The yttrium(III) complex of 1,4,7,10-tetraazacyclododecane-1,4,7,10-tetraacetic acid (YDOTA) was prepared as a sodium salt as previously described.[19] The yttrium content of each batch of YDOTA was determined by ICP-MS (Galbraith Laboratories). The trityl radical tris{8-carboxyl-2,2,6,6-benzo(1,2-d:4,5-d)-bis(1,3)dithiole-4-yl}methyl sodium salt (OX063) was obtained from Oxford Instruments Molecular Biotools, while 4-oxo-2,2,6,6-tetramethypiperidine-1-oxyl (TEMPO) and 4-oxo-2,2,6,6-tetramethypiperidine-d_{16}-1-oxyl (TEMPO-d_{16}) were both obtained from Sigma-Aldrich. All other chemicals and solvents were obtained from commercial sources and were used without further purification.

Dynamic Nuclear Polarization (DNP) of YDOTA. The YDOTA samples were prepared for DNP by dissolving YDOTA in the appropriate glassing agent to obtain a saturated solution and then doped with the paramagnetic species. Prior to microwave irradiation, the samples (40 μL) were quickly frozen in liquid nitrogen to ensure glass formation. The DNP was performed using an Oxford HyperSense commercial polarizer following previously published procedures.[9,19,21] The frozen sample was immediately inserted into the HyperSense polarizer (1.4 K) then irradiated with microwaves (100 mW) at a frequency near the ESR frequency (approximately 94 GHz at 3.35 T) of the radical. After 5−9 h of polarizing time, 4 mL of superheated water was injected into the sample holder and 3.5 mL of solution was transferred into a 10 mm NMR tube in a 9.4 T high resolution magnet via a Teflon tube with a transfer time t_{tr} of 8 s for ^{89}Y NMR spectrum acquisition.

Liquid-State NMR Enhancement Calculation. The NMR signal intensity serves as a "thermometer" of spin temperature T_s of the nuclear spin system.[23,24] Here the NMR signal enhancement is defined as $\varepsilon = P_{hp}/P_{th}$ where P_{hp} is the DNP-enhanced polarization corresponding to a spin temperature T_s and expressed as $P_{hp} = \tanh(h\nu_n/2k_BT_s)$ while P_{th} is the thermal polarization at a given lattice temperature T_L and written as $P_{th} = \tanh(h\nu_n/2k_BT_L)$. Experimentally, the liquid-state NMR signal enhancement ε is determined by calculating the ratio of the integrated area of the T_1-corrected hyperpolarized (HP) signal A_{hp} over the thermal equilibrium NMR signal A_{th}:

$$\varepsilon = (A_{hp}/A_{th})(\sin\theta_{th}/\sin\theta_{hp})(c_{th}/c_{hp})\exp(t/T_1) \qquad (1)$$

where the subscripts hp and th denote the parameters measured in the hyperpolarized and thermal equilibrium states, respectively. The ratio $(\sin\theta_{th}/\sin\theta_{hp})$ denotes the rf flip angle correction factor while (c_{th}/c_{hp}) is the concentration correction factor to ensure that the ratio of the signal intensity in both states are based on equal spin count. Typically, a 90-degree flip angle is used to get the spectra on both states so the correction factor $(\sin\theta_{th}/\sin\theta_{hp})$ is unity. As described previously, 40 μL aliquots of sample are used for solid-state polarization; the solid-state concentration is diluted to 3.5 mL in the liquid-state, so the dilution factor is 1/88. The ^{89}Y NMR signal measured in a 3 M YCl_3 aqueous solution was used as the reference thermal signal since no thermal ^{89}Y NMR signal could be detected from the diluted dissolution liquids even after several hundred acquisitions. The factor $\exp(t/T_1)$ accounts for the loss of the hyperpolarized NMR signal due to relaxation during the dissolution transfer with $t = t_{tr} = 8$ s. However, the effect of the T_1-correction factor on the ^{89}Y enhancement is negligible due to the very long T_1 of the nucleus, and therefore, it was ignored.

Nuclear Spin−Lattice Relaxation Time (T_1) Measurement. YDOTA samples (160 μL) were polarized for 2 h using a method described previously. The polarized sample was diluted to 3.5 mL solution after dissolution (dilution factor of 1/22). One milliliter of the dissolved liquid was immediately placed in a 10 mm NMR tube where the sample volume is within the NMR coil. The decay of the hyperpolarized signal was monitored by taking a spectrum with 10° rf pulse every 30 s. All liquid-state T_1 measurements were done in a 9.4 T magnet at 298 K.

Co-Polarization of YDOTA and Sodium [1-^{13}C]Pyruvate. A solution of YDOTA (0.14 M) and sodium [1-^{13}C]pyruvate (0.75 M) in 1:1 glycerol/water was doped with trityl OX063 radical (15 mM) and ProHance (2.5 mM). Then, 40 μL aliquots were polarized as described previously.

RESULTS AND DISCUSSION

Thermal Mixing. The maximum attainable nuclear polarization is determined by the dominant mechanism of DNP. The two main mechanisms of DNP are *thermal mixing* and the *solid effect*; their contribution to the overall nuclear polarization enhancement strongly depends on the experimental conditions such as the applied field of the polarizer, temperature, and the EPR properties of the paramagnetic species.[3,5] A brief qualitative discussion of these processes will aid the interpretation of the results of this work. The microwave-driven transfer of the polarization of the electrons to the nuclear spins can be thermodynamically described by the thermal interaction of three systems: (*i*) the nuclear Zeeman, (*ii*) electron Zeeman, and

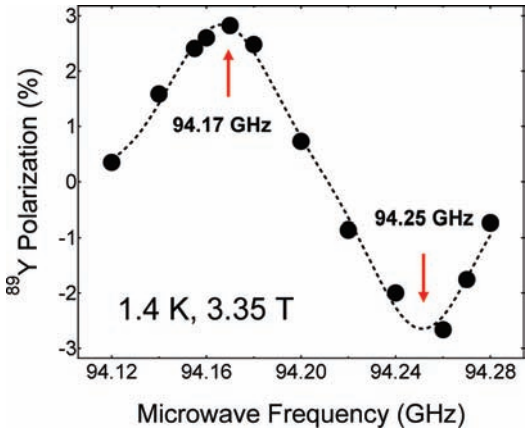

Figure 1. ^{89}Y polarization of the yttrium complex of 1,4,7,10-tetraazacyclododecane-1,4,7,10-tetraacetic acid (DOTA) (0.28 M in 1:1 vol/vol glycerol/water doped with 15 mM OX063 trityl radical) as a function of microwave frequency. The up and down arrows indicate the positive and negative polarization peaks, respectively. Each data point represents a separate DNP experiment.

(*iii*) the electron spin−spin interaction (SSI) reservoirs.[3−5,26,27] If the EPR linewidth of the radical *D* is comparable to the nuclear Larmor frequency ν_n and the concentration of the paramagnetic species is high enough to maintain strong electron dipolar interactions, then the electron SSI and the nuclear Zeeman reservoirs are "thermally coupled" and polarization transfer is achieved by thermal mixing mechanism.[3,27] Thermal mixing occurs in two consecutive steps:[5,27] first, the electron SSI reservoir is cooled by the electron Zeeman system whose spin temperature is lowered due to the microwave-driven reduction of the effective magnetic field seen by the electrons in a reference frame rotating with the rf magnetic field.[25] This process is analogous to the adiabatic demagnetization described by the Redfield theory.[28,29] In the second step, two electrons perform a flip-flop transition in an energy-conserving process releasing a quantum of energy $\hbar\omega$ that excites a nuclear transition, lowering the spin temperature of the nuclear spins. As a result, the electrons and all nuclear species achieve a common spin temperature, T_s under microwave irradiation. On the other hand, when ν_n is significantly greater than *D*, then the nuclear Zeeman and electron SSI reservoirs are "thermally decoupled" and instead of thermal mixing, the DNP proceeds via the so-called solid effect. This mechanism involves one electron and one nuclear spin and arises from the microwave excitation of forbidden transitions involving both spins simultaneously. Since the probability of the forbidden transitions is low, the solid effect is much less efficient than thermal mixing.[3,27,30]

The Microwave DNP Spectrum of ^{89}YDOTA. The frequency of the applied microwave radiation is one of the most important parameters in microwave-driven DNP. Typically, the dependence of the solid-state nuclear polarization or NMR signal enhancement on the microwave irradiation frequency (the microwave DNP spectrum) follows a curve with a maximum and minimum located downfield and upfield of the EPR resonance frequency of the paramagnetic polarizing agent, respectively. These frequency values correspond to the highest positive and negative nuclear polarization (see Figure 1). Obviously, these frequency values should be used in the DNP experiment to obtain the highest signal enhancement. Experimentally, for ^{13}C-labeled compounds, the microwave sweep is easily performed using the tunable built-in NMR coil of the polarizer. However, in our case, the solid-state ^{89}Y NMR signal could not be detected because of spurious NMR ringing signals which are dominant at the low NMR frequency of ^{89}Y and the low temperature of the DNP. This forced us to measure the liquid-state NMR enhancements for each data point of the ^{89}YDOTA microwave frequency sweep (Figure 1) in a separate sample.

These values represent the polarization 8 s after dissolution due the transfer from the polarizer to the magnet. However, because of the long T_1 of ^{89}YDOTA, there is only a negligible loss of polarization during the transfer of the dissolution liquid. The microwave sweep of ^{89}YDOTA (Figure 1) in the presence of the trityl OX063 radical is very similar to that of ^{13}C-labeled pyruvate with nearly the same separation of positive and negative polarization peaks (see Figure S1 in Supporting Information).

The microwave DNP spectrum also offers the possibility of deducing the underlying mechanism of DNP. Theoretically, a high temperature approximation of the density matrix describing the DNP process is given by the Provotorov theory;[3,31] however, it should be pointed out that the Provotorov equations are not valid at the operating temperature of the HyperSense polarizer (1.4 K). A qualitative description of the DNP at this temperature is provided by the Borghini model,[3,25] which is derived from the Redfield theory (see a brief description of the Borghini model in the Supporting Information). Simulations of ^{13}C-labeled samples doped with trityl OX063[32] and TEMPO[33] radicals at 3.35 T using the Borghini model revealed that the computed polarization values are generally higher than the experimental data, an indication that the model is incomplete and needs to incorporate several factors involved in the experimental setup. Nevertheless, the Borghini approximation provides an acceptable qualitative description of the microwave DNP spectrum and correctly predicts one of the most characteristic feature of thermal mixing, namely, the maximum positive and negative enhancements of all nuclei in the thermal mixing regime ($D \geq \nu_n$), are achieved at the same microwave frequency.[25] Previous DNP experiments with ^{13}C and ^{15}N labeled urea in the presence of a trityl radical using the HyperSense polarizer have shown that the underlying mechanism of DNP is thermal mixing for both of these nuclei. Therefore, considering the extremely low Larmor frequency ν_n of ^{89}Y, we anticipated that thermal mixing is the dominant mechanism for ^{89}Y DNP as well. This was confirmed by the experimental data (Figure 1), which show no or negligible contribution from the solid effect. If the underlying mechanism of ^{89}Y DNP were the solid effect,[3,30] then the polarization peaks would be separated by $2\nu_n$ = 14 MHz which is not the case here.

The Dependence of ^{89}Y DNP on the ESR Linewidth. Experimental data in the literature for deuteron DNP have shown that, within the thermal mixing regime, nuclear polarization levels are higher when radicals with narrower ESR linewidths are used.[34,35] We observed a similar trend when the effect of ESR linewidth on the ^{89}Y enhancement was studied. YDOTA samples were polarized in glycerol/water matrix in the presence of free radicals with markedly different ESR linewidth: trityl OX063, 4-oxo-TEMPO, and 4-oxo-TEMPO-d_{16} (Chart 2. The optimal frequency for DNP with nitroxides was determined using a 4-oxo-TEMPO-doped sodium [1-^{13}C]pyruvate sample (see Figure S2).

The carbon-centered trityl OX063 has the narrowest ESR linewidth (full-width half-maximum $D \sim 63$ MHz[34]) among these three radicals because its paramagnetic central carbon atom

dx.doi.org/10.1021/ja201880y |*J. Am. Chem. Soc.* 2011, 133, 8673–8680

is surrounded by $I = 0$ nuclei to eliminate hyperfine coupling and the broadening due to g anisotropy is suppressed by its symmetrical structure.[34] In contrast, the ESR linewidth of nitroxyl radicals is around 6−10 times wider than that of trityl under DNP conditions.[36] The main source of line broadening in nitroxyls is the g-anisotropy and the interaction of the unpaired electron with the ^{14}N and ^{1}H nuclei. On the basis of literature data,[37,38] deuteration of the C−H bonds in nitroxyl decreases the linewidth about half at low field (X-band, 23 °C) but the effect is much less at higher field. It should be noted, however, that it is quite difficult to give a definitive linewidth for nitroxyl radicals because the ESR spectrum changes dramatically with field strength and temperature.

As expected, the trityl radical gave the highest ^{89}YDOTA enhancements (Table 1). While the nitroxyl radicals (4-oxo-TEMPO, 4-oxo-TEMPO-d_{16}) did not perform as well as the trityl OX063, they did produce considerable nuclear polarization enhancement. Samples doped with the deuterated nitroxyl radical derivative 4-oxo-TEMPO-d_{16} worked slightly better than the undeuterated 4-oxo-TEMPO owing to the weaker hyperfine interaction of the paramagnetic electron with deuterons (γ_n = 6.54 MHz/T) than with protons (γ_n = 42.577 MHz/T). The dependence of polarization on the EPR linewidth can be understood based on the thermodynamic treatment of thermal mixing: the heat capacity of the non-Zeeman electron reservoir is given by $C_{nZ} = NAD^2$ where N is the number of electrons, A is the proportionality constant, and D is the EPR linewidth that includes all homogeneous and inhomogeneous line broadening effects originating from variations in the local magnetic field and can, therefore, be written as $D^2 = \gamma_e(B_{hom}^2 + B_{inh}^2)$.[35] The inhomogeneous contribution to the ESR linewidth originating from hyperfine interactions and g-anisotropy can be more than an order of magnitude larger than the homogeneous contribution for nitroxyl radicals. Since dynamic cooling of the electron dipole−dipole reservoir by the microwave irradiation and, consequently, thermal mixing is more efficient when the heat capacity of this reservoir is smaller, radicals that have a narrow ESR linewidth with small or no inhomogeneous contribution to the line broadening should produce higher nuclear polarization.[34,35] The spin−lattice relaxation times of YDOTA samples doped with nitroxyl radicals have slightly lower values because of the higher concentration of paramagnetic agents present in the liquid state (Figure S3). For practical purposes, nitroxyls as polarizing agents for ^{89}Y, ^{15}N, or ^{13}C can be considered as a less costly alternative to trityl although lower nuclear polarizations are achieved.

Chart 2. Free radical polarizing agents used in this work

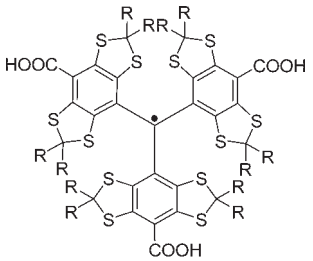

The Effect of the Glassing Agent. The composition of the frozen matrix is a key parameter for DNP. One of the necessary conditions for efficient thermal mixing is strong dipole−dipole interactions between electron spins that resonate at different frequencies in the ESR spectrum. In general, this requires an isotropic glass matrix, in which the orientation of the molecules is uncorrelated. In addition, both the compound to be polarized and the free radical must be soluble in the glassing agent. We have studied various water−glassing agent mixtures for the DNP of YDOTA (water, DMSO, methanol, 1,3-propanediol, ethylene glycol, 18-crown-6, and glycerol) and the enhancement data are shown in Table 1.

The viscous glass formers such as ethylene glycol, glycerol, 18-crown-6, and 1,3-propanediol gave the best ^{89}Y polarization. Surprisingly, a small enhancement was observed using pure water despite an expected formation of crystalline matrix. A possible explanation for this interesting observation may involve the formation of regions of amorphous ice when a droplet of saturated YDOTA solution is rapidly cooled.[39] The wide range of NMR enhancements obtained in different glassing matrices (Table 1), with values ranging from 2000 to 20 000, suggests that

Table 1. Summary of the Dependence of Room-Temperature Liquid-State ^{89}Y NMR Enhancement on the Choice of Glassing Agents and Radicals[a]

glassing matrix	radical/conc (mM)	YDOTA (M)	enhancement	% polarization
Pure water	Trityl/15	0.48	2200	0.35
Glycerol/water	Trityl/15	0.28	17700	2.79
Glycerol/water	TEMPO/40	0.28	4600	0.73
Glycerol/water	TEMPO-d_{16}/40	0.28	5400	0.85
18-Crown-6/water	Trityl/15	0.27	20400	3.22
Ethylene glycol/water	Trityl/15	0.24	12600	1.99
DMSO/water	Trityl/15	0.24	2900	0.46
1,3-propanediol/water	Trityl/15	0.24	18500	2.92
Methanol/water	Trityl/15	0.24	3000	0.47

[a] The NMR enhancements ($N = 3$) were measured in a 9.4 T magnet at 298 K after dissolution of samples polarized for 9 h at 1.4 K and 3.35 T. Maximum soluble concentration of Y-DOTA were used in different glassing agents mixed with 50% water by volume. The error bar in the enhancement is within 5−8%.

dx.doi.org/10.1021/ja201880y | J. Am. Chem. Soc. 2011, 133, 8673–8680

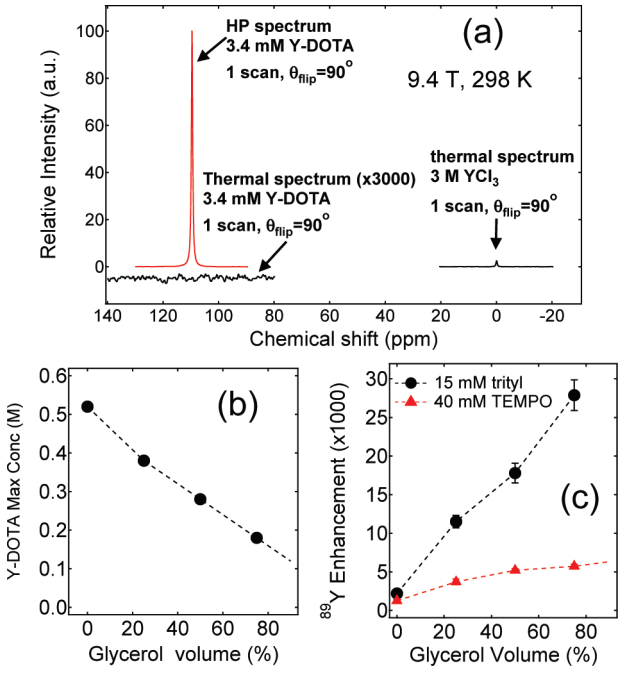

Figure 2. (a) Relative ^{89}Y liquid-state NMR signal at 9.4 T and 298 K in the hyperpolarized (HP) and thermal states (3.4 mM) and thermal signal from aqueous YCl_3 sample (3 M). (b) Maximum YDOTA concentration in varying glycerol volume percent in aqueous solution. (c) Corresponding liquid-state NMR enhancement of samples ($N = 3$) doped with trityl and TEMPO as a function of varying glycerol volume in water.

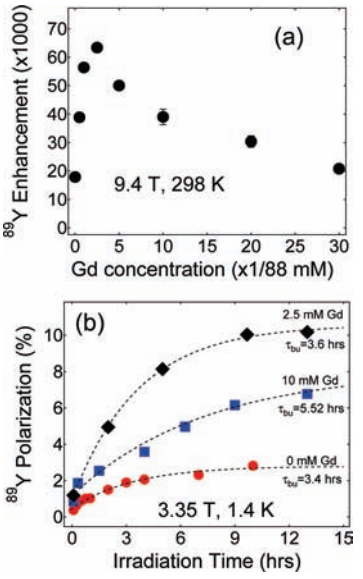

Figure 3. Effect of Gd(III) doping. (a) Room-temperature liquid-state NMR enhancement as a function of Gd doping in the solid-state. The dilution factor of the Gd concentration after dissolution is 1/88. Maximum enhancement is achieved with 2.5 mM Gd doping. Each data point represents an average of three separate DNP experiments. (b) Polarization buildup curves of 0.28 M YDOTA samples in 1:1 glycerol/water glassing matrix doped with 15 mM trityl and Gd (0, 2.5, and 10 mM). Each data point represents a separate DNP experiment.

the nuclear polarization of the target solute is highly dependent on the microscopic properties of the glassing matrix.[40] We have selected glycerol as the preferred glass former for subsequent optimization measurements because it is compatible with planned *in vivo* experiments. Another important observation is that the ^{89}Y NMR signal enhancement monotonically increased with increasing glycerol content in water but this comes at the expense of lower solubility of YDOTA (see Figure 2b,c). This implies that the DNP of YDOTA is more efficient in glassing mixtures with high glycerol content. For practical applications, however, it is more advantageous to produce concentrated solutions of hyperpolarized compounds and so a glassing matrix composed of 1:1 (v/v) glycerol/water appears to be optimal since this affords relatively high NMR enhancement and reasonably high hyperpolarized YDOTA concentrations. It is interesting to note that, among the glassing agents we have tried, the water/18-crown-6 mixture produced the highest ^{89}Y NMR signal enhancement. While using a crown ether as a glassing agent for biomedical purposes is not practical, one may speculate whether the formation of Na^+−18-crown-6 complexes play a role in the DNP, for example, by preventing the formation of Na^+-$[YDOTA]^-$ ion pairs. The ^{23}Na has a spin of 3/2 and a quadrupole moment of 104 mb and may affect the solid state relaxation times. Assuming a logK of 0.8 for the thermodynamic stability of Na[18-crown-6], in a glassing mixture containing 25% crown ether, about 90% of the Na^+ ions is complexed by 18-crown-6.[41]

The Effect of Gd(III) Relaxation Agent. Earlier studies demonstrated that the presence of trace amount of a T_1 relaxation agent such as $GdCl_3$ or a Gd(III)-complex increases the solid state polarization of ^{13}C-labeled compounds.[15,32] This observation prompted us to study the effect of the relaxation agent ProHance (gadolinium complex of 10-(2-hydroxy-propyl)-1,4,7,10-tetraazacyclododecane-1,4,7-triacetic acid) (Chart S1) on the nuclear polarization enhancement of YDOTA.

Addition of ProHance to an YDOTA sample doped with 15 mM trityl radical in a 1:1 glycerol/water matrix dramatically improved the ^{89}Y polarization buildup: over 3-fold increase in the enhancement at 9.4 T and 298 K, from 18 000 to 65 000, was observed at the optimal concentration of ProHance (2.5 mM). Higher concentrations of ProHance reduced the polarization level dramatically (Figure 3a). The ^{89}Y polarization buildup as a function of time was measured in the presence and absence of ProHance (Figure 3b). The lines represent fits to the exponential equation:

$$P(t) = P_0 + P_{max}[1\text{-}\exp(-t/\tau_{bu})] \quad (3)$$

where P_0 is the baseline, P_{max} is the maximum polarization achieved, and τ_{bu} is the polarization buildup time constant. The slower polarization buildup is in the presence of the Gd-complex probably reflects the relaxation-enhancing effect of Gd(III) on the solid-state nuclear T_1 of ^{89}Y spins (Figure 3b).

Since the liquid-state ^{89}Y T_1 relaxation time can also be affected by the Gd(III), the T_1 relaxation time of ^{89}YDOTA was measured in Gd(III) containing samples. Figure 4a shows the liquid-state T_1 decay of hyperpolarized ^{89}Y from YDOTA samples with different Gd(III) concentration. The T_1 values were obtained by the fitting of hyperpolarized NMR signal decay to eq 4 that also includes the effect of radiofrequency (rf) pulsing with a given flip angle θ:[42]

$$M_z(t) = M_0 \sin\theta(\cos\theta)^{t/TR} \exp(-t/T_1) \quad (4)$$

where TR is the repetition time and M_0 is the original magnetization before the rf pulse.

dx.doi.org/10.1021/ja201880y |J. Am. Chem. Soc. 2011, 133, 8673–8680

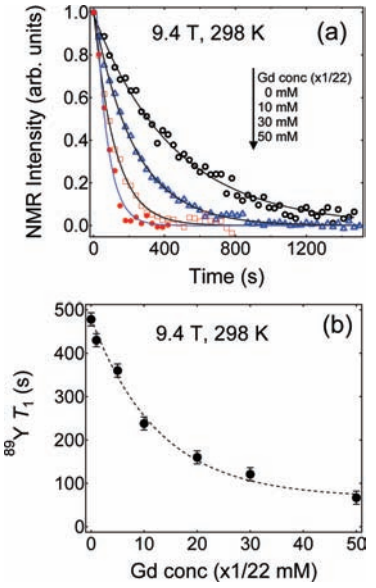

Figure 4. (a) Decay of hyperpolarized ^{89}Y NMR signal of YDOTA samples doped with different Gd concentrations (dilution factor of concentration from solid-state to liquid-state is 1/22). The solid lines are fits to eq 4. Each point corresponds to the integrated spectral area taken every 30 s with a 5° flip angle. Each curve represents a separate DNP experiment. (b) Liquid-state state T_1 as a function of Gd doping. Each data point represents an average of three separate DNP experiments.

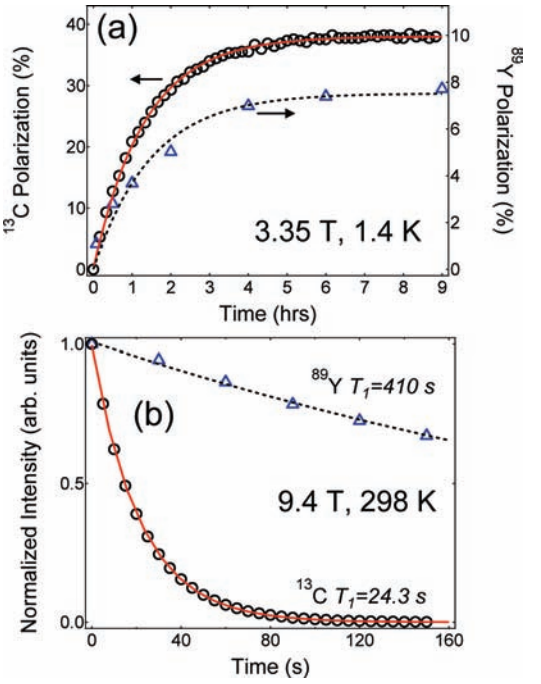

Figure 5. Co-polarization of ^{13}C and ^{89}Y spins: (a) Polarization buildup of samples with [1-^{13}C]pyruvate (left axis) and ^{89}YDOTA (right axis) doped with 15 mM trityl OX063 and 2.5 mM Gd(III) at 1.4 K and 3.35 T. Each data point in the ^{89}Y buildup curve represents a separate DNP experiment. (b) Decay of hyperpolarized ^{13}C (θ_{flip} = 2 deg, TR = 5 s) and ^{89}Y (θ_{flip} = 10 deg, TR = 30 s) NMR signals at room temperature after dissolution.

It should be noted that at the optimal Gd(III) concentration (2.5 mM) the liquid state T_1 of ^{89}Y is only slightly reduced; however, as expected, at higher concentrations the T_1 shortening effect of Gd(III) becomes more pronounced (Figure 4b).

The ^{89}Y nuclear polarization enhancing effect of Gd(III) can be understood by considering its effect on the spin temperature. Maximum polarization is attained when the spin temperature is at minimum (eq 5). Under DNP conditions, the minimum spin temperature can be predicted using eq 6:[34]

$$P_{max} = \tanh(\mu B/k_B T_{s,min}) \quad (5)$$

$$T_{s,min} = \frac{2DT_L\sqrt{\eta(1+f)}}{\omega_e} \quad (6)$$

where D is the ESR linewidth,f is the nuclear relaxation leakage factor and η the ratio of the electronic Zeeman and dipolar relaxation rates (T^Z_{1e}/T^D_{1e}).[34] From thermodynamic point of view, $1/T^Z_{1e}$ is the heating rate of the dipolar reservoir and $1/T^D_{1e}$ is the cooling rate of the electron Zeeman reservoir.[35] To achieve the minimum spin temperature of the nuclear Zeeman system, the electron Zeeman system should be strongly coupled to the lattice (short T^Z_{1e}) while the electron dipolar system has to be weakly coupled to the lattice (long T^D_{1e}).[35] It is likely that the presence of a Gd(III) relaxation agent shortens the Zeeman T^Z_{1e} of the free radical thus reducing the ratio η. This leads to a lower T_s and consequently higher nuclear polarization level. This is in agreement with reported experimental data which show that the (Zeeman) electronic relaxation time of the trityl OX063 radical is dramatically shortened by $GdCl_3$ where at 3.35 T and 1.2 K the T_{1e} of trityl is close to 1 s and was reduced by almost one-third with the addition of 1 mM Gd(III).[32] Addition of Gd(III) above 2.5 mM in the solid-state sample leads to longer polarization buildup times (Figure 3a) and lower polarization levels, which may be attributed to the competition of polarization buildup and spin−lattice relaxation of nuclear spins.

Heteronuclear Co-Polarization of ^{89}YDOTA and Sodium [1-^{13}C]Pyruvate. To further establish thermal mixing as the main DNP mechanism for ^{89}Y and to directly compare the effect of Gd(III) relaxation agent on the polarization buildup and T_1 values of ^{89}Y and ^{13}C, we performed an experiment in which ^{89}YDOTA and sodium [1-^{13}C] pyruvate were co-polarized in the presence of ProHance. In thermal mixing, ^{89}Y and ^{13}C nuclear spins should acquire the same spin temperature even in the presence of Gd(III). Samples containing YDOTA (0.14 M), sodium [1-^{13}C]pyruvate (0.75 M), and ProHance (2.5 mM) in glycerol/water (1:1) were polarized using trityl OX063 radical (15 mM) as polarizing agent. The ^{13}C polarization buildup (Figure 5a) was followed using the built-in solid state NMR probe of the HyperSense polarizer while the ^{89}Y polarization was measured in the liquid state after dissolution and transfer. Each data point in the ^{89}Y polarization buildup curve in Figure 5a represents a separate DNP experiment. The data collected in this experiment provides a strong evidence for thermal mixing between the nuclear species ^{89}Y and ^{13}C and the dynamically cooled SSI reservoir. When the ^{13}C polarization achieved 37.3%, the ^{89}Y polarization was 7.72%. These polarization levels correspond to a common spin temperature of $T_s(^{89}Y) = T_s(^{13}C) \approx 2.2$ mK in the solid state (calculated using eq 5).

The ^{89}Y and ^{13}C enhancement data at each time point in Figure 5 are in excellent agreement with the equal spin temperature (EST) prediction of the Borghini model indicating that at all times during microwave irradiation both nuclear spin species share the same spin temperature. This nicely corroborates with

dx.doi.org/10.1021/ja201880y |J. Am. Chem. Soc. 2011, 133, 8673–8680

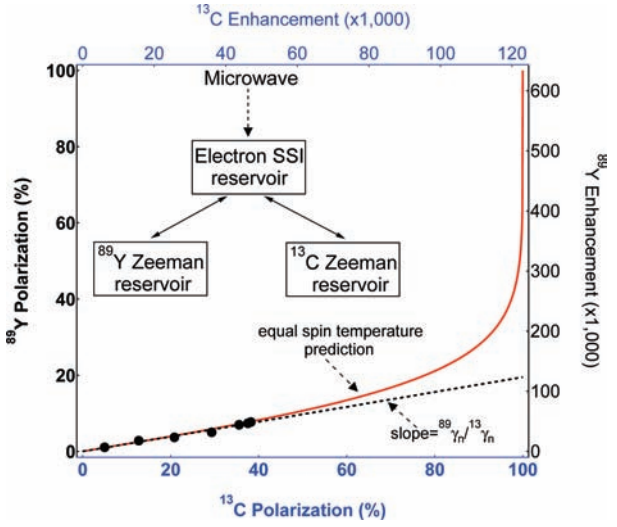

Figure 6. ^{89}Y (left axis) versus ^{13}C (bottom axis) polarization plotted with spin temperature T_s as the implicit parameter. The data points were taken from Figure 5. The mirror axes correspond to the ^{89}Y and ^{13}C NMR signal enhancement at 9.4 T and 298 K. The solid line is the thermal mixing prediction (eq 6) where both nuclear spin species acquire the same T_s in the solid-state under microwave irradiation and the dashed line is from the fit $P(^{89}\text{Y}) = (^{89}\gamma_n/^{13}\gamma_n)P(^{13}\text{C})$. Inset: Thermal mixing model where the ^{89}Y and ^{13}C nuclear Zeeman reservoirs are in thermal contact with the electron spin−spin interaction reservoir which is dynamically cooled by microwave irradiation.

the established observation[26,43,44] that the thermal mixing time of nuclear Zeeman reservoirs with the electron SSI reservoir is an extremely fast process relative to the nuclear polarization buildup time.

We also determined the liquid state spin−lattice relaxation times of both nuclei in this set of experiments. The liquid-state ^{13}C T_1 of pyruvate sample doped with ProHance was found to be around 24.3 s (298 K, 9.4 T), significantly shorter than the reported T_1 (47 s at 11.7 T and 67 s at 3 T). The ^{89}Y T_1, in accordance with T_1 measurements discussed earlier, was not affected significantly. These results are not surprising since the relaxation effect of Gd(III) is mediated by dipolar interactions and therefore, proportional to the gyromagnetic ratio of the nucleus. The decay of hyperpolarized ^{13}C and ^{89}Y NMR signals are shown in Figure 5b and the significantly slower decay of the ^{89}Y signal clearly demonstrates the advantage of a long T_1 value in preserving the polarization.

The challenge of polarizing low γ_n nuclei is well illustrated in Figure 6, which is a plot of the ^{89}Y polarization versus ^{13}C polarization with spin temperature (irradiation time) as the implicit parameter. Since in thermal mixing the nuclei have equal spin temperature, $T_s(^{89}\text{Y}) = T_s(^{13}\text{C})$, the ^{89}Y polarization $P(^{89}\text{Y})$ can be expressed as a function of ^{13}C polarization $P(^{13}\text{C})$:

$$P(^{89}\text{Y}) = \tanh[(^{89}\gamma_n/^{13}\gamma_n)\tanh^{-1}(P(^{13}\text{C}))] \qquad (7)$$

In the low polarization limit, this equation reduces to the linear $P(^{89}\text{Y}) \approx (^{89}\gamma_n/^{13}\gamma_n)P(^{13}\text{C})$. The graph in Figure 6 predicts that, for example, in order to achieve an ^{89}Y polarization of 30%, one must be able to polarize ^{13}C to 92%. To the best of our knowledge, the highest ^{13}C polarization level reported in the literature is around 40−60%.[6,45,46] The right and top scales of Figure 6 show the room-temperature ^{89}Y and ^{13}C NMR enhancements that correspond to these polarizations in a 9.4 T magnet. The theoretical NMR signal enhancement for fully polarized samples (P = 100%) at 9.4 T and 298 K is 613 000 for ^{89}Y and 123 000 for ^{13}C. Thus, there is room for improvement and, since the spin temperature of DNP-enhanced nuclear spins is directly proportional to the lattice temperature (eq 6), further increases in nuclear polarization could be achieved by lowering the T_L below 1.4 K. The reported working base temperature of current home-built DNP polarizers is close to 1.0 K.[6,33,47] Obviously, decreasing the lattice temperature down to the millikelvin range using ^{3}He cryogenic systems and dilution refrigerators[35] would result in even higher polarization levels, but a number of engineering challenges would have to be addressed to incorporate the fast dissolution device in such a polarizer. The advantage of lowering the lattice temperature has been demonstrated in deuteron polarization studies where polarization levels as high as 81%[35] have been achieved at T_L = 150 mK and 2.5 T using trityl OX063 radical as the paramagnetic agent (these polarizers did not include a dissolution system). The maximum ^{2}H polarization level achieved under these conditions corresponds to a spin temperature $T_s \approx 0.44$ mK at 2.5 T. Another possible method to increase the nuclear polarization is performing the DNP in stronger magnetic field, which theoretically leads to lower spin temperature as depicted in eq 6. However, experiments on ^{2}H polarization via thermal mixing in deuterated butanol samples doped with TEMPO and paramagnetic Cr(V)-based polarizing agents showed that increasing the field above 3.5 T lead to lower polarization due to the strong response of the g-anisotropy of these radicals with increasing magnetic field.[35]

CONCLUSION

In summary, we have achieved ^{89}Y polarization levels up to 10%, which corresponds to 65 000-fold enhancement of the thermal NMR signal at room temperature in a 9.4 T magnet. The increase of ^{89}Y polarization level was achieved through (*i*) establishing the optimal microwave irradiation frequency, (*ii*) optimizing the glassing matrix, (*iii*) choosing a radical with negligible inhomogeneous line broadening contribution to the ESR linewidth, and (*iv*) addition of an electron T_{1e} relaxation agent. Heteronuclear co-polarization experiments of ^{89}YDOTA and sodium [1-^{13}C]pyruvate unequivocally established thermal mixing as the underlying mechanism of DNP for these nuclei. Addition of a T_{1e} relaxation agent resulted in a dramatic increase in both the ^{89}Y and ^{13}C polarization levels and, as expected, had only a small effect on the T_1 relaxation time of the ^{89}Y nucleus. The DNP optimization details here are vital for obtaining higher enhancements for future *in vivo* imaging applications using hyperpolarized ^{89}Y complexes. The methodology to optimize nuclear polarization as described here may also be applicable for enhancing the DNP signals of other NMR-active nuclei.

ASSOCIATED CONTENT

Supporting Information. A brief discussion of the Borghini model, ^{13}C microwave DNP spectra of trityl and TEMPO-doped sodium [1-^{13}C]pyruvate, and liquid-state nuclear T_1 decay curve for TEMPO-doped YDOTA samples. This material is available free of charge via the Internet at http://pubs.acs.org.

AUTHOR INFORMATION

Corresponding Author
zoltan.kovacs@utsouthwestern.edu

ACKNOWLEDGMENT

This work is supported by the National Institutes of Health grant numbers 1R21EB009147-01 and RR02584.

REFERENCES

(1) Slichter, C. P. *Principles of Magnetic Resonance*; Springer: New York, 1989.
(2) Abragam, A. *Principles of Nuclear Magnetism*; Oxford University Press: England, 1961.
(3) Abragam, A.; Goldman, M. *Rep. Prog. Phys.* **1978**, *41*, 395–467.
(4) de Boer, W. *J. Low Temp. Phys.* **1976**, *22*, 185.
(5) Crabb, D. G.; Meyer, W. *Annu. Rev. Nucl. Part. Sci.* **1997**, *47*, 67.
(6) Ardenkjaer-Larsen, J. H.; Fridlund, B.; Gram, A.; Hansson, G.; Hansson, L.; Lerche, M. H.; Servin, R.; Thaning, M.; Golman, K. *Proc. Natl. Acad. Sci. U.S.A.* **2003**, *100*, 10158–10163.
(7) Day, S. E.; Kettunen, M. I.; Gallagher, F. A.; Hu, D. E.; Lerche, M.; Wolber, J.; Golman, K.; Ardenkjaer-Larsen, J. H.; Brindle, K. M. *Nat. Med.* **2007**, *13*, 1382–1387.
(8) Golman, K.; in't Zandt, R.; Thaning, M. *Proc. Natl. Acad. Sci. U.S. A.* **2006**, *103*, 11270–11275.
(9) Merritt, M. E.; Harrison, C.; Storey, C.; Jeffrey, F. M.; Sherry, A. D.; Malloy, C. R. *Proc. Natl. Acad. Sci. U.S.A.* **2007**, *104*, 19773–19777.
(10) Chen, A. P.; Albers, M. J.; Cunningham, C. H.; Kohler, S. J.; Yen, Y. F.; Hurd, R. E.; Tropp, J.; Bok, R.; Pauly, J. M.; Nelson, S. J.; Kurhanewicz, J.; Vigneron, D. B. *Magn. Reson. Med.* **2007**, *58*, 1099–1106.
(11) Gallagher, F. A.; Kettunen, M. I.; Brindle, K. M. *Prog. Nucl. Magn. Reson. Spectrosc.* **2009**, *55*, 285.
(12) Golman, K.; in't Zandt, R.; Lerche, M.; Pehrson, R.; Ardenkjaer-Larsen, J. H. *Cancer Res.* **2006**, *66*, 10855–10860.
(13) Gabellieri, C.; Reynolds, S.; Lavie, A.; Payne, G. S.; Leach, M. O.; Eykyn, T. R. *J. Am. Chem. Soc.* **2008**, *130*, 4598–4599.
(14) Marsjanska, M.; Iltis, I.; Shestov, A. A.; Deelchand, D. K.; Nelson, C.; Ugurbil, K.; Henry, P. R. *J. Magn. Reson.* **2010**, *206*, 210–218.
(15) Wilson, D. M.; Keshari, K. R.; Larson, P. E. Z.; Chen, A. P.; Hu, S.; Van Criekinge, M.; Bok, R.; Nelson, S. J.; Macdonald, J. M.; Vigneron, D. B.; Kurhanewicz, J. *J. Magn. Reson.* **2010**, *205*, 141–147.
(16) Karlsson, M.; Jensen, P. K.; in't Zandt, R.; Gisselson, A.; Hasson, G.; Duus, J. O.; Meier, S.; Lerche, M. H. *Int. J. Cancer* **2010**, *127*, 729–736.
(17) Cudalbu, C.; Comment, A.; Kurdzesau, F.; van Heeswijk, R. B.; Uffman, K.; Jannin, S.; Denisov, V.; Kirik, D.; Gruetter, R. *Phys. Chem. Chem. Phys.* **2010**, *12*, 5818–5823.
(18) Gallagher, F. A.; Kettunen, M. I.; Hu, D.-E.; Jensen, P. R.; In't Zandt, R.; Karlsson, M.; Gisselson, A.; Nelson, S. K.; Witney, T. H.; Bohndlek, S. E.; Hansson, G.; Peltersen, T.; Lerche, M. H.; Brindle, K. M. *Proc. Natl. Acad. Sci. U.S.A.* **2009**, *106*, 19801–19806.
(19) Merritt, M. E.; Harrison, C.; Kovacs, Z.; Kshirsagar, P.; Malloy, C. R.; Sherry, A. D. *J. Am. Chem. Soc.* **2007**, *129*, 12942–12943.
(20) Holz, R. C.; Horrocks, W. D., Jr. *J. Magn. Reson.* **1990**, *89*, 627–631.
(21) Jindal, A. K.; Merritt, M. E.; Suh, E. H.; Malloy, C. R.; Sherry, A. D.; Kovacs, Z. *J. Am. Chem. Soc.* **2010**, *132*, 784–785.
(22) Mieville, P.; Jannin, S.; Helm, L.; Bodenhausen, G. *J. Am. Chem. Soc.* **2010**, *132*, 5006–5007.
(23) Bloembergen, N.; Purcell, E. M.; Pound, R. V. *Phys. Rev.* **1948**, 73679.
(24) Abragam, A.; Proctor, W. G. *Phys. Rev.* **1958**, *109*, 1441.
(25) Borghini, M. *Phys. Rev. Lett.* **1968**, *20*, 419–421.
(26) Borghini, M.; Scheffer, K. *Phys. Rev. Lett.* **1971**, *26*, 1362.
(27) Goertz, S. T. *Nucl. Instrum. Methods* **2004**, *526*, 28–42.
(28) Redfield, A. G. *Phys. Rev.* **1955**, *98*, 1787–1809.
(29) Redfield, A. G. *Science* **1969**, *164*, 1015–1523.
(30) Borghini, M. *Phys. Rev. Lett.* **1966**, *16*, 318.
(31) Provotorov, B. N. *Sov. Phys. JETP* **1962**, *14*, 1126–1131.
(32) Ardenkjaer-Larsen, J. H.; Macholl, S.; Johanesson, H. *Appl. Magn. Reson.* **2008**, *34*, 509–522.
(33) Jannin, S.; Comment, A.; Kurdzesau, F.; Konter, J. A.; Hautle, P.; van der Brandt, B.; van der Klink, J. J. *J. Chem. Phys.* **2008**, *128*, 241102–241104.
(34) Heckmann, J.; Meyer, W.; Radtke, E.; Reicherz, G.; Goertz, S. *Phys. Rev. B* **2006**, *74*, 134418.
(35) Goertz, S. T.; Harmsen, J.; Heckmann, J.; Heb, Ch.; Meyer, W.; Radtke, E.; Reicherz, G. *Nucl. Instrum. Methods* **2004**, *526*, 43–52.
(36) Heckmann, J.; Goertz, S. T.; Meyer, W.; Radtke, E.; Reicher, G. *Nucl. Instrum. Methods Phys. Res., Sect. A* **2004**, *526*, 110–116.
(37) Radner, F.; Rassat, A.; Hersvall, C. *J. Acta Chim. Scand.* **1996**, *50*, 146–149.
(38) van der Brandt, B.; Bunyatova, E. I.; Hautle, P.; Konter, J. A. *Nucl. Instrum. Methods Phys. Res., Sect. A* **2004**, *526*, 53–55.
(39) Debenedetti, P. G. *J. Phys.: Condens. Matter* **2003**, *15*, R1669–R1726.
(40) Kurdzesau, F.; van den Brandt, B.; Comment, A.; Hautle, P.; Jannin, S.; van der Klink, J. J.; Konter, J. A. *J. Phys. D: Appl. Phys.* **2008**, *41*, 155506.
(41) Arnaud-Neu, F.; Delgado, R.; Chaves, S. *Pure Appl. Chem.* **2003**, *75*, 71–102.
(42) Patyal, B. R.; Gao, J. H.; Williams, R. F.; Roby, J.; Saam, B.; Rockwell, B. A.; Thomas, R. J.; Stolarski, D. J.; Fox, P. T. *J. Magn. Reson.* **1997**, *126*, 58–65.
(43) de Boer, W.; Borghini, M.; Morimoto, K.; Niinikoski, T. O.; Udo, F. *J. Low Temp. Phys.* **1974**, *15*, 249.
(44) Goldman, M.; Cox, S. F. J.; Bouffard, V. *J. Phys. C: Solid State Phys.* **1974**, *7*, 2940–2952.
(45) Wolber, J.; Ellner, F.; Fridlund, B.; Gram, A.; Johannesson, H.; Hansson, G.; Hansson, L.; Lerche, M. H.; Mansson, S.; Servin, R.; Thaning, M.; Golman, K.; Ardenkjaer-Larsen, J. H. *Nucl. Instrum. Methods Phys. Res., Sect. A* **2004**, *526*, 173–181.
(46) Johannesson, H.; Macholl, S.; Ardenkjaer-Larsen, J. H. *J. Magn. Reson.* **2008**, *197*, 167–175.
(47) Comment, A.; van der Brandt, B.; Uffman, K.; Kurdzesau, F.; Jannin, S.; Konter, J. A.; Hautle, P.; Wenkebach, W. T.; Gruetter, R.; van der Klink, J. J. *Concepts Magn. Reson., Part B* **2007**, *31*, 255–269.